High Velocity Impact on generic CFRP blade specimen: baseline free method for impact localisation and damage assessment on complex structures.

Stefano Cuomo[a], Tim Bätzel[b], Niels Modler[b], Andreas Hornig[b], Michele Meo[a]

[a]Department of Mechanical Engineering, University of Bath, Bath, BA2 7AY, UK

[b]Technische Universität Dresden, Institute of Lightweight Engineering and Polymer Technology (ILK), Holbeinstraße 3, 01307 Dresden, Germany

*m.meo@bath.ac.uk;

ABSTRACT

Nowadays components made of UD composite materials are largely diffused in many engineering fields, such as automotive, railways, marine and aerospace. Main drawback of this class of materials lies in their low out-of-plane properties making them very sensible to impulsive loads such as impact events. After a collision with an external object, composites structures could be affected by damage, sometimes not visible from visual inspections (barely visible damage - BVID) hence with detrimental consequences on structure resistance and strength. Therefore, it is fundamental in terms of safety to continuously assess the healthy state of structures during their life and determine whether an impact event has occurred and if it caused damage or not. This work proposes a baseline free methodology to determine the coordinates of very high velocity impact on complex structures and evaluate if damage has occurred during the impact by only acquiring signal during the impact event. The technique overcomes the common limitations of previous technique presented in literature, i.e., a priori knowledge of mechanical properties, vibration response analysis, wave propagation direction dependency, sensor locations. The routine developed is based first on the estimation of the power of the acoustic emission generated by impact events, at sensors location, then the power information through the entire structure is reconstructed exploiting radial basis function network. The actual impact estimation is finally obtained using a weighted method. Furthermore, damage assessment is conducted with a novel method based on Hilbert Huang transform and mode decomposition. Experimental tests were performed on a generic CFRP blade specimen with a complex stacking sequence and embedded sensors. Two test configurations at different velocities were considered: one at 90 m/s and one at 190 m/s. Before and afterwards the actual impact tests, the blade was excited as well with a modal hammer (pre and post impact). The results from the impact analysis highlighted the validity and reliability of the proposed method, with a high level of accuracy in terms of impact localisation estimation, and qualitative integrity state was effectively evaluated.

Keywords: Impact localization, BVID, Embedded transducers, very high velocity impact, complex structures, Radial basis functions, Signal power method, Composite materials.

1. INTRODUCTION

The necessity to assess the integrity state of structures is fundamental in most of the engineering applications, they could be in automotive, marine, railways, but it is in aerospace where "health" monitoring was introduced and is still developed as a priority activity. Structural Health Monitoring (SHM) is "the process of acquiring and analysing data from on-board sensors to evaluate the health of a structure" as defined by the SAE standard ARP6461 [1]. The aim is to continuously evaluate and detect mechanical loads affecting the structure during the life cycle and determine whether structural damage has occurred due to extreme conditions. The output information from the monitoring process informs the inspection activities leading to reduced maintenance costs in terms of resources and time, hence improving aircraft availability, a strong competitive factor for flight operators.

The SHM usually follows two different approaches: active SHM; and passive SHM [2] [3]. In active SHM transducers induce ultrasonic waves through the structure assessing the structural state, detecting any eventual damage. The methods used in the active approach are similar to the ones used in non-destructive evaluation (NDE). The main limitation of this methodology is the low feasibility to inspect large structures, e.g., aircraft, resulting in time-consuming operations. It is necessary therefore an early detection methodology to specifically direct the inspection on the area of interest. This task is possibly exploiting the passive SHM. Indeed, any impact, crack initiation and propagation or failure are a source of acoustic waves, that could be detected and acquired using acoustic sensors. This process is defined as source localization, and once has been performed and the region of interest identified, further analysis with active SHM could be executed in order to investigate the presence of damage.

This work focuses on the development of a source localisation technique for high velocity impact, overcoming the limitations of previous methods. Hence, before introducing the proposed tool, a review of the methods existing in literature is discussed.

Generally, waves are disturbances that propagate from one region to another [4]. An impact event induces the propagation of acoustic waves within the affected structure, with the creation of transient elastic waves generated by the redistribution of the stress field [5]. There are multiple types of mode for waves propagating in solids, such as pressure waves, shear waves, flexural, Rayleigh and Lamb waves. Each of them is associated to a specific particle motion that define the wave propagation, e.g., in longitudinal waves the motion is parallel to the direction of the wave propagation, or in shear waves the particle motion is perpendicular to the wave propagation direction. Within the SHM applications, research focused the attention towards ultrasonic guided waves (UGW), defined as elastic disturbances that can propagate in thin walled structures with very little loss of amplitude [2], [6]. The main types of guided waves are shear waves (vertical and horizontal), Lamb and Rayleigh waves, all propagating confined through structures with distinct boundaries. Usually, when structural components are characterized by large overall dimension to thickness ratio values, the propagation mode is described by Lamb waves. For high frequency-thickness products, there is a transition to Rayleigh waves (surface waves) [7]. Usually, multiple sensors are used to detect and acquire the propagating waves through the structure, and commonly these are piezoelectric transducers, being small, lightweight, low cost and can be attached onto the surfaces or embedded in the structure itself.

It is of primary importance to determine the location of the impact event that a structure could face, as mentioned before, in order to direct the inspection procedure effectively. In literature multiple methods and technique based on the acoustic emission (AE) have been proposed, using different approaches to evaluate the position of the impact, that is seen as the acoustic source of the propagating waves within the structure.

One of the first proposed tools to evaluate the impact location was the triangulation method, commonly applied to plate like isotropic structures, made of homogeneous materials and well know wave speed direction dependency [8]. This method needs an accurate evaluation of the wave speed, and small variations badly affect the localization results.

When the wave speed is unknown, optimization techniques have been proposed, for both isotropic and anisotropic structures [9], with higher accuracy increasing the number of sensors. Different authors [10], [11] proposed and developed the beamforming technique for isotropic plates, and others [12], [13] extended it to anisotropic structures as well. This technique is sensitive to sensors configuration on the inspected structure, and moreover

for the anisotropic solution the knowledge of direction-dependent wave velocity is required. A localization method for anisotropic structures with arbitrary cross-section and unknown properties was developed [14], [15] solving a set of non-linear equations combining local and global optimisation methods. In [16] exploiting cluster of sensors, and the time differences of the acquired signals, the localization is obtained from the intersection of the straight lines (wave direction) tracked from the cluster of sensors. Hence, more clusters lead to increased resolution. If the acoustic source is close to one of the sensor clusters, the error in the prediction is higher, and this specific cluster should be ignored in the calculation. A localization method for both isotropic and anisotropic structures without a-priori knowledge of mechanical properties, was developed on the optimal sensors configuration, allowing the linearization of well-known nonlinear system of equations and based on the Akaike Information Criterion (AIC) for the estimation of the time of arrival [17].

A different approach, overcoming the a-priori knowledge of material properties, structure geometry and characteristics, is the Time Reversal (TR) method [18]. The localization is obtained in two steps, the first being the acquisition of the structural response on a set of points on the structure, then, the second, performing the cross-correlation of the previous recorded signals with the actual impact event [19]–[21]. The area enclosing the maximum correlation coefficient is the "impact cell", and then the actual impact coordinates are determined with topological method, e.g. gravity method [22], [23], or minimum average (MA) [24].

All the mentioned techniques are affected by different limitations, indeed some of them are effective only for isotropic and homogeneous materials and when the wave speed direction dependency is well known. Other techniques are affected by the sensors configuration and require a relatively large number of receivers. Some techniques rely on the time of arrival estimation and different methods to evaluate it are used. The time of arrival is very sensible to the nature of the propagating wave, being very keen to alteration, inducing poor estimations of the actual value. Other methods are designed on the generation of a baseline of the structural responses, process that could be very time consuming.

In this work a new method is proposed that is based on the direct evaluation of the power of the propagating elastic waves through the structure. With this novel localization technique, the knowledge of materials characteristics and properties, the wave speed dependency, time of arrival estimation is not required. Moreover, this method does not require a baseline, and hence is effective for both real time and remote localization estimations.

2. POWER METHOD

The proposed method is designed on the signal power calculation of the propagating waves through the monitored structure. It is essential for the proposed tool, a distributed set of receiving sensors to properly determine the power distribution in the structure or component. Exploiting the power of signals an early work developed a system identification method for impacts [25]. Other works on the power method were focused on the localization on composite plate-like structures [26] and on damage detection and localization with induced ultrasonic waves [27]. The developed tool is based on a similar approach to these last two works. The novelty in this research resides on the refinement the method in order to be reliable applied to complex structures. Indeed, the tested sample in this work was a generic CFRP blade specimen with a complex stacking sequence and embedded piezo transducers. Furthermore, very high velocities have been chosen for the test campaign while previous works limited to low velocity impact.

The starting point of the localization process is the signal acquisition via the distributed set of sensors. After the impact event, the redistribution of the stress filed triggers the propagation of elastic waves through the structure. When the wave reaches the receivers, a set of signals, one for each sensor, is acquired with proper sampling frequency and stored. The higher the number of available signals, hence more receiving sensors, the better is the estimation of the power distribution on the structure.

Let's consider the generic acquired signal, *s(t)*, from one of the piezo transducers. The energy of the signal is defined as the following:

$$E(t) = \int_{t_0}^{t_f} |s(t)|^2 dt \tag{1}$$

With $t_f - t_0$ representing the time window selected for the energy calculation.

From Eq. (1) it's straightforward to calculate the power value of the given signal. Considering the same time window previously introduced, power of a signal *s(t)*, is defined by the following:

$$P(t) = \frac{1}{t_f - t_0}\int_{t_0}^{t_f} |s(t)|^2 dt \tag{2}$$

Gathering all the signals from the available sensors, and for each of them calculating the power with Eq. (2), it is possible to determine the power distribution of the impact event. Instead of manual time window selection as found in previous works, in this paper a threshold method was introduced. The time frame of interest, within evaluate the power values of each sensor, was determined by a routine that calculates the time when the signal maximum amplitude is reduced by 50%. Of all the signal acquired from the available sensors, the one with the highest amplitude is considered to select the time window. This improved time window feature can automate the localisation process, which in turn can be performed in real time on structures of any complexity.

The power values so far calculated refers to the sensor's locations, so it is more a discrete mapping of power values rather than a proper distribution. To obtain a smooth and continuous power distribution, an interpolation process among the power values calculated is executed. The interpolation method used in this work is the radial basis function (RBF) method, characterised by good performance for scattered data and good level of smoothing [28], hence suitable to interpolate data with complex trend, as in the case of the experimental setup considered in this work. With this method, the interpolant function among the known power values is given by the following:

$$p(\boldsymbol{r}) = \sum_{i=1}^{N} \lambda_i \phi \|\boldsymbol{r} - \boldsymbol{r_i}\| + \sum_{j=1}^{M} b_j p_j(\boldsymbol{r}) \tag{3}$$

Where ϕ is the radial basis function or kernel, cantered in $\boldsymbol{r_i}$, where the power values are known; $\|\boldsymbol{r} - \boldsymbol{r_i}\|$ is the Euclidian norm, λ_i weight coefficients and b_j scalar parameters of the polynomial term $p_j(\boldsymbol{r})$ [29]–[31].

The term ϕ needs to be a function radially symmetric in each $\boldsymbol{r_i}$, and the system must be well-posed, ensuring non-singularity. This is obtained using the $\|\boldsymbol{r} - \boldsymbol{r_i}\|$ term, because from linear algebra a matrix with Euclidian distance as terms, for distinct points in $\mathbb{R}^n$ is always non-singular, hence there exists a unique interpolation function. The radial basis function should be continuous with its derivatives, ideally $C^\infty$to be a good interpolation function. The basis function that has been chosen in this work is the thin plate spline, defined by the following:

$$\phi(\boldsymbol{r}) = \boldsymbol{r^2}\ln(\boldsymbol{r}) \tag{4}$$

for smoothness properties and continuity in the first derivative terms (C^1), ensuring interpolation conditions for the known values. Moreover, this function, compared to other radial basis functions (gaussian, multiquadric, inverse quadratic) needs not shape parameter tuning. The low order polynomial term in Eq. (3) is added in order to guarantee the unique existence of the interpolant function [22], [28].

Eq. (3) is a linear combination of basis function and a polynomial term; hence it is possible to use the matrix form and linear algebra to find the interpolating function, solving a system of linear equations. The interpolating function is given by the following:

$$\begin{bmatrix} A & P \\ P^T & 0 \end{bmatrix} \begin{bmatrix} \lambda \\ b \end{bmatrix} = \begin{bmatrix} p \\ 0 \end{bmatrix} \tag{5}$$

A is the interpolating matrix, *P* is the coordinates matrix and p is the vector of the known power values. From this system we evaluate the weight coefficients (λ_i, b_j) related to the radial basis function, thus:

$$\begin{bmatrix} \lambda_i \\ \vdots \\ \lambda_N \\ b_1 \\ b_M \\ b_0 \end{bmatrix} = \begin{bmatrix} \phi_{1,1} & \cdots & \phi_{1,N} & x_1 & y_1 & 1 \\ \vdots & \ddots & \vdots & \vdots & \vdots & \vdots \\ \phi_{N,1} & \cdots & \phi_{N,N} & x_N & y_N & 1 \\ x_1 & \cdots & x_N & 0 & 0 & 0 \\ y_1 & \cdots & y_N & 0 & 0 & 0 \\ 1 & \cdots & 1 & 0 & 0 & 0 \end{bmatrix}^{-1} \begin{bmatrix} p_1 \\ \vdots \\ p_N \\ 0 \\ 0 \\ 0 \end{bmatrix} \tag{6}$$

With the known p_n power values, we obtain the expansion or weight coefficients, then substituting in Eq. (3) the power values in the M unknown coordinates trough interpolation. Finally, a finer and smooth power distribution is obtained.

With the entire power distribution obtained, it is possible to perform the actual impact localization exploiting a topological process such as the gravity method:

$$x_k = \frac{\sum_{k=1}^{M+N} x_k P_k}{\sum_{k=1}^{M+N} x_k} \qquad y_k = \frac{\sum_{k=1}^{M+N} y_k P_k}{\sum_{k=1}^{M+N} y_k} \tag{7}$$

Finally estimating the coordinates of the impact event on the tested component. The output is plotted on a schematic representation of the sample generated by the algorithm itself, including actual impact location mark to appreciate the estimation performance of the method.

To compare the localization results with the actual impact, the accuracy is defined in terms of distance, hence:

$$\Lambda = \sqrt{(x_{real} - x_{estimated})^2 + (y_{real} - y_{estimated})^2} \tag{8}$$

with x_{real}, y_{real} actual impact coordinates and $x_{estimated}$, $y_{estimated}$ the estimated coordinates given in output by the tool.

3. MANUFACTURING

A generic CFRP blade specimen was manufactured using a prepreg stacking process, where a planar middle surface and double curved cross-section was chosen to produce two components within one manufacturing process. The materials used were HexPly M90 and M21 unidirectional (UD) prepreg, with high performance very though epoxy matrix for aerospace applications. For further compliance, the entire manufacturing process was performed under aviation quality control standards with a seamless documentation of all relevant parameters. A stacking sequence composed of 61 full size plies and additional 47 wedge-plies in the root area enables a near net shape preforming. The corresponding mould with the blade specimen and the manufacturing process is illustrated in Figure 1.

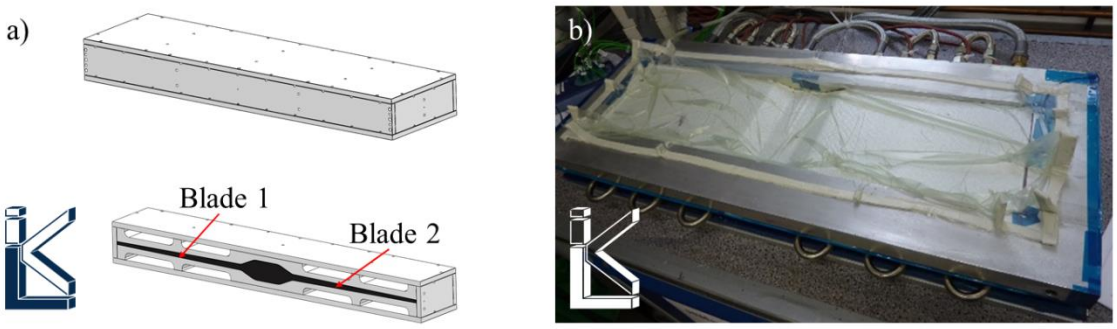

Figure 1. Curing mould geometry (a); preforming mould during compaction (b)

A tailored embeddable sensor-actuator layer (TEmSAL) was integrated between the 58th and 59th layer, close to the pressure side surface, facing away from the impact (Figure 2). The TEmSAL consists of two polyimide films with printed conduction paths and six piezo elements embedded in between. More detailed information concerning the TEmSAL manufacturing can be found in [32] , [33] and [34].

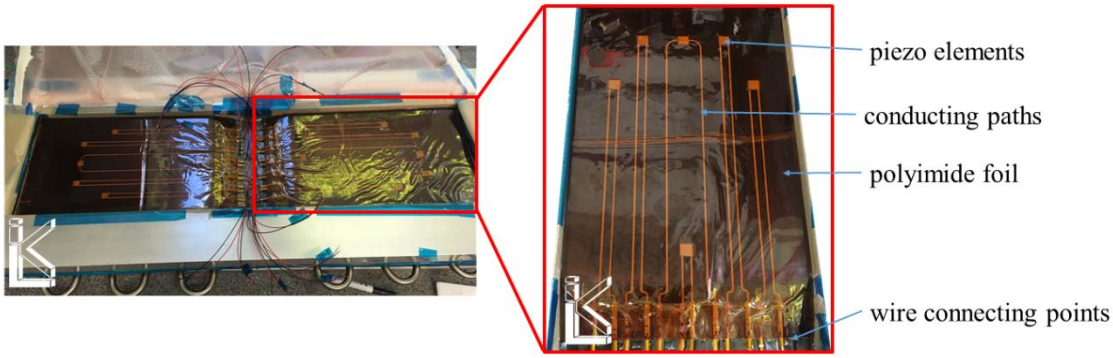

Figure 2. TEmSAL in the preforming mould during stacking process

Ceramic piezo elements (PZT 5A1, L x W x T: 10x10x0.2 mm) were used for this purpose. The piezo elements were contacted to allow the measurement of piezoelectric charges over the elements thickness (stacking direction in the laminate, top and bottom surfaces are contacted). The piezo elements were positioned where the locations of the highest strains in the first four eigenmodes (Figure 3) are expected according to preliminary finite element analysis. An additional reinforcement laminate has been bonded to the leading and trailing edges after the autoclave consolidation process for edge protection purposes during the impact event. Before stacking and after consolidation and confectioning, the piezo elements were polarised for 120 s with a voltage of 360 V.

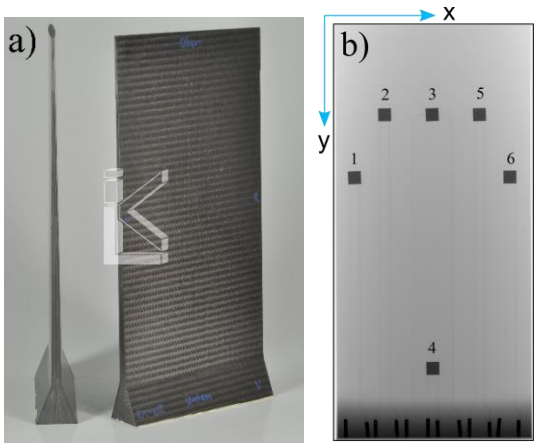

Sensors configuration		
Number	x [mm]	y [mm]
1	15	125
2	38	67
3	75	67
4	75	268
5	112	67
6	135	125

Figure 3. Consolidated generic blade specimen (a) and CT-scan (b) and sensors coordinates.

4. EXPERIMENTAL SETUP

A cylindrical impactor (ballistic gelatine type 3, length of 60 mm, diameter of 20 mm) was used to mimic a bird strike event on the down scaled generic blade specimen. Two high-speed cameras (25k fps) were installed for a top and side view of the impact event (Figure 4). Signals of the piezo elements were measured at a rate of 5 MS/s. Since high strains and therefore high voltage signals were expected, additional scaling-capacitors (100 nF and 330 nF) were connected in parallel to each piezo element to scale the signals amplitude down to a maximum value that is compatible with the data acquisition system (17.5V threshold of the AD-converter unit). The capacitance value was estimated on the basis of previous preliminary impact test experiments [30].

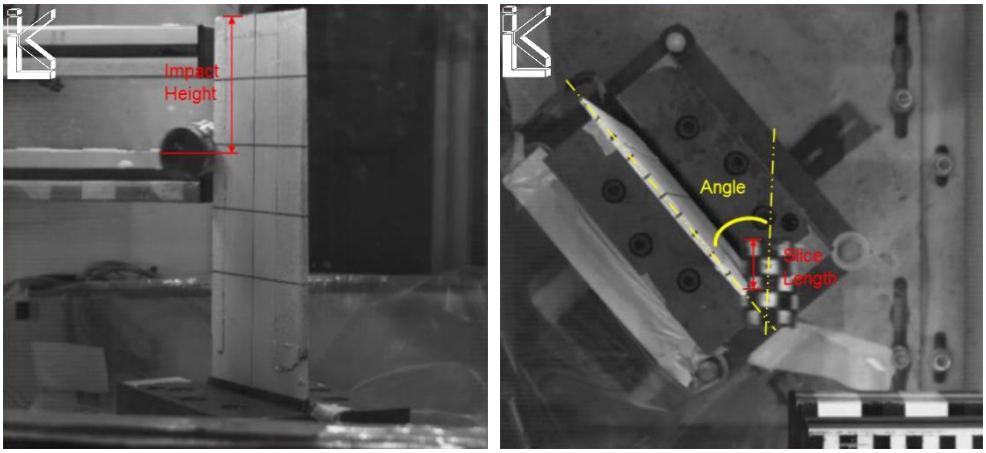

Figure 4. High-speed views of impact experiments with metrics for specimen alignment.

For the impact test configuration, the generic blade specimen was positioned with a stagger angle of 40° with respect to the ballistic trajectory for the impactor to hit the leading edge at a height of 106 mm with a slice length of 34 mm (Figure 4). The root was fully constrained through a clamping mechanism. A schematic overview of the test configuration is given in Figure 5.

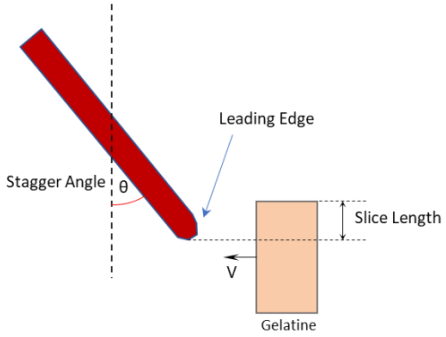

Figure 5. Impact test configuration.

Two impact experiments with impactor velocities of 90 m/s and 190 m/s were conducted using the same generic blade specimen. Before and after the impact with the gelatine the blade was tested by exciting it with a modal impact hammer in two different locations, as in the detail depicted in Figure 6. Then, the blade was tested at two different energy levels, the first with a projectile velocity of 90 m/s and the second with projectile velocity of 190 m/s. Both scenarios, pre and post analysis with instrumented hammer were executed. Hence, the complete test campaign was, as synthesised as follow, in Table 1:

Impact Test	
90 m/s	190 m/s
Pre analysis (hammer)	Pre analysis (hammer)
Impact (gelatine block)	Impact (gelatine block)
Post analysis (hammer)	Post analysis (hammer)

Table 1 – Test executed during the experimental campaign.

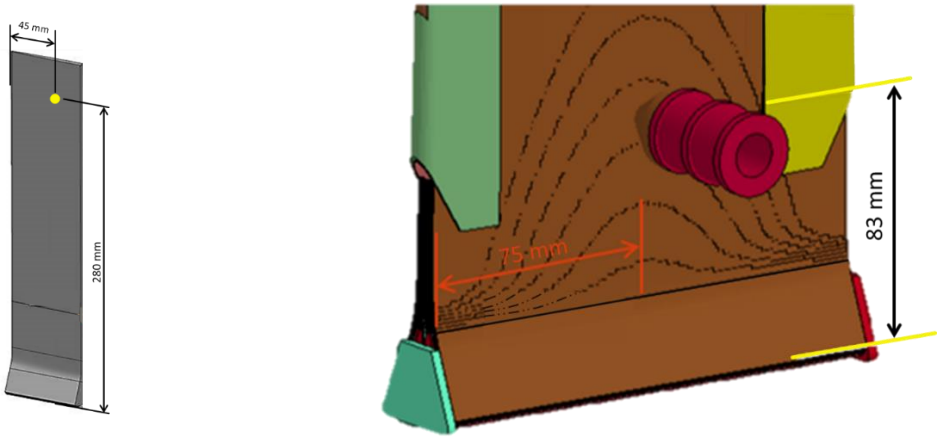

Figure 6. Post analysis impact location details: pre/post 90 m/s (left); pre/post 190 m/s (right).

5. IMPACT TEST RESULTS

Results from experimental campaign are here reported and discussed. This paragraph is divided into two sections, one for 90 m/s impact and one for 190 m/s. The accuracy level performed by the algorithm is defined by the localisation error Λ from Eq. (8) and introduced in chapter 3. Dataset from the test campaign was processed and elaborated, to correctly feed the algorithm with a proper set of data to be then analysed.

5.1. Impact test: 90 m/s

The first impact test was performed at 90 m/s, that falls in the high velocity impact range. It is worth noting that high velocities are defined as impact with a velocity range from 50 m/s and above. Intermediate velocity impact (IVI) is between 20 m/s and 50 m/s, and below 10-20 m/s are defined as low velocity impact (LVI) [35]. Different definitions of impact velocities are proposed in the literature [36], [37] but in general, the aforementioned ranges are valid.

Figure 6 illustrates the impact test at 90 m/s. During the stage of direct contact between impactor and generic blade specimen a combination of cantilever bending, and torsional deformation is observed. After separation of impactor and specimen until the end of signal logging, a sustained oscillation with bending and torsional components was present.

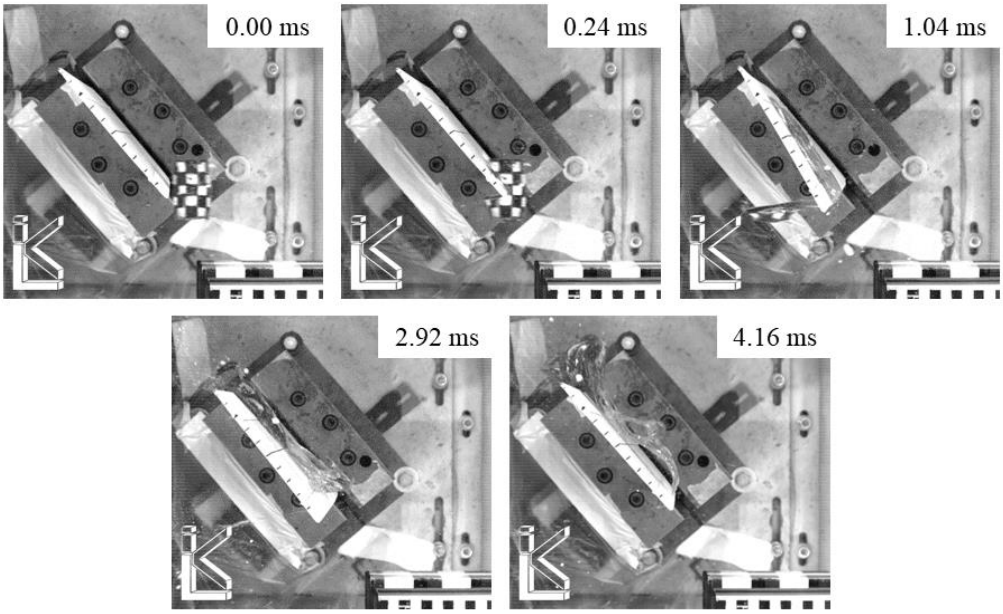

Figure 7. Impact test at 90 m/s.

For the impact experiment at 90 m/s, the voltage signal was measured across scaling capacitances of 100 nF. Piezo element 5 was not functional during the first test, which is implied by the unexpectedly low signal maximum of 0.05 V (Figure 6). The remaining piezo elements delivered a high voltage, low noise signal while piezo elements 2-4 overshot the measurable range close to the impact beginning.

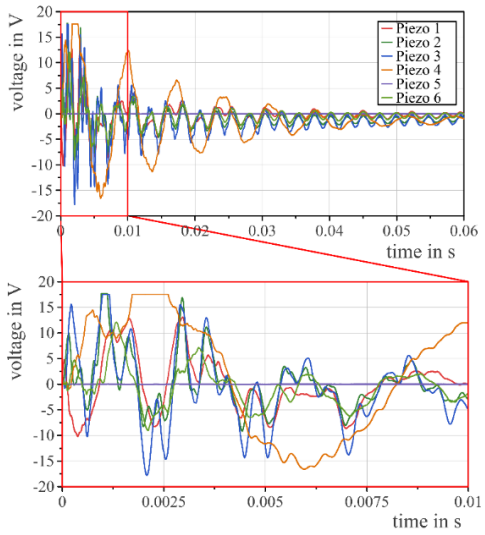

Figure 8. Signals of piezo elements during impact test at 90 m/s.

Measurements before and after the first impact test revealed no significant change of the piezo element's capacitance, which indicates that no failure occurred during the impact at 90 m/s.

Processing dataset from the impact at 90 m/s, the channel number four (piezo 5) was measured but due to malfunction of the sensor its data were omitted from the calculation in all scenarios (pre/impact/post). For this reason, in the following pictures the failed sensor will not be reported.

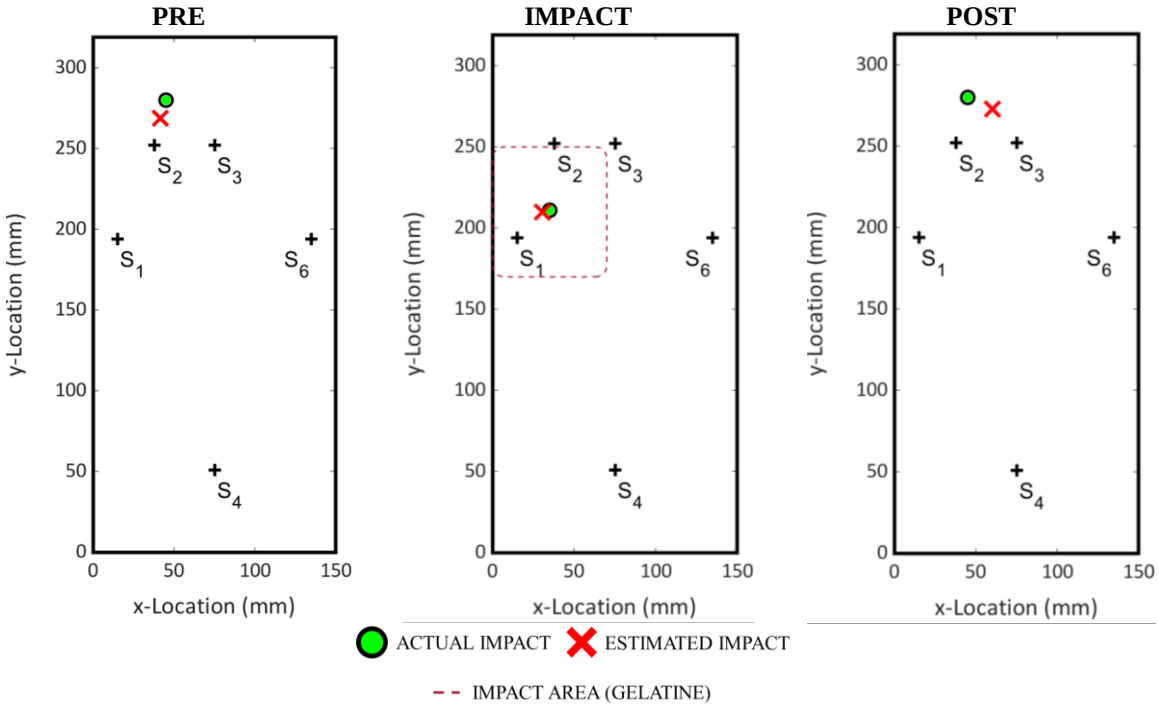

Figure 9. Impact location estimation 90 m/s, pre analysis (**PRE**), impact with gelatine (**IMPACT**) and post analysis (**POST**).

The estimation of impact location, using data acquired during blade excitation with instrumented hammer shows excellent accuracy (Λ = 11.60 mm), with five piezo sensors operating out of six. Processing data from the impact executed with high velocity gelatine projectile, the estimation is accurate (Λ = 4.61 mm), with coordinates very close to the actual impact location, as depicted in Figure 8. Performing the post analysis impact, the localisation error increases slightly compared to PRE and IMPACT, but still a good level of accuracy (Λ = 16.73 mm).
Considering the geometry complexity and the energy level of the impact, the estimation given in output by the algorithm is accurate. The increased error seen in post analysis should not be related to any specific detriment or damage of the sensing system or data acquisition unit, neither by damage within the sample itself, as confirmed by the piezo elements capacitance measured before and after the test revealing no significant changes. These results confirm the possibility to embed piezo transducers within complex structures designed for high performance tasks (e.g., engine blade), and continuously inspect and verify any possible impact with foreign objects with a simple but effective localisation method as the proposed one. Considering the faulty sensor, more research should focus on the manufacturing process and how a robust embedded sensing layer can be achieved.

5.2. Impact test: 190 m/s

During the impact at 190 m/s the generic CFRP blade specimen exhibited an oscillation deformation behaviour comparable to the one in the 90 m/s test, consisting of bending and torsional portions. Due to the higher impact velocity, higher deformation amplitudes and frequencies were observed. Because of the effective sudden acceleration during the impact, the edge protection of the trailing edge de-bonded (Figure 10).

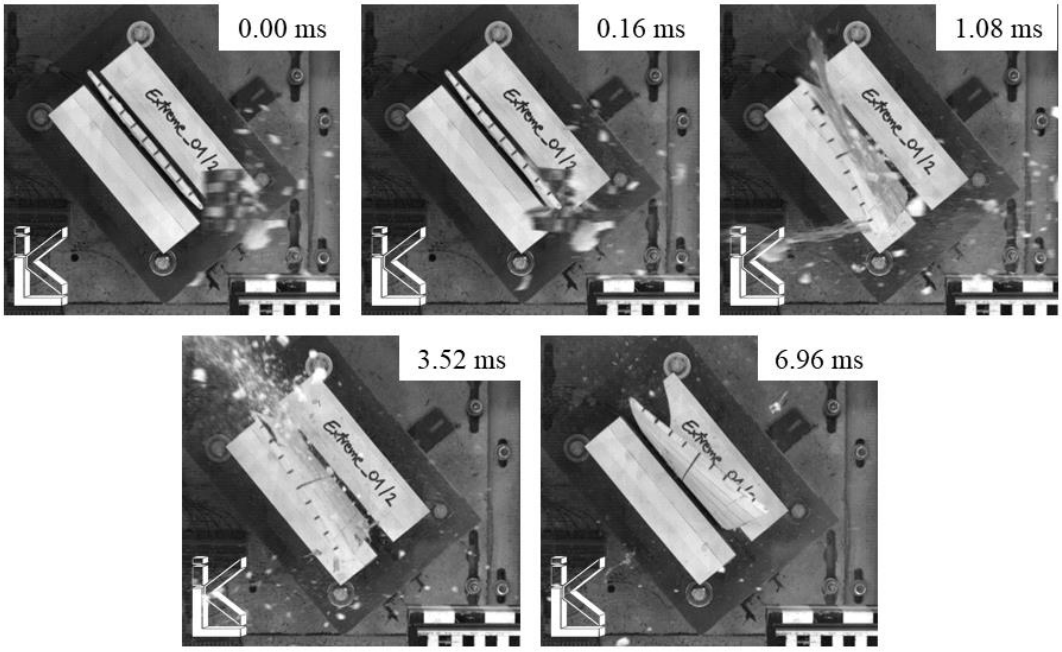

Figure 10. Impact test at 190 m/s.

The scaling-capacitances were raised to 330 nF before the experiment to further prevent signal overshoots caused by the higher impact-velocity. Therefore, the signals from Figure 10 need to be scaled by a factor of 3.3 for direct comparison to the results of the impact at 90 m/s (Figure 8).

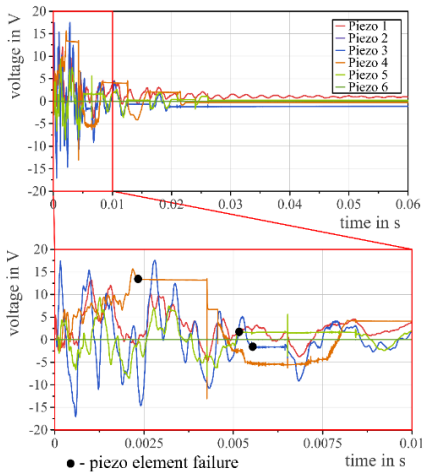

Figure 11. Signals of piezo elements during impact test at 190 m/s.

It was found that piezo elements 2 and 6 were not working prior to the second impact test. Piezo element 3, 4 and 5 failed during impact. The exact time of failure for each piezo element is marked with a black dot in Figure 11. Capacitance measurements prior and past the second impact test confirmed the failure of said piezo elements.

The second scenario was at 100 m/s higher than the first impact and the specimen was the same as the previous test. Processing the signals acquired during the pre-testing, channel 5 (sensor 6) was measured but connected to the hammer loadcell, so was excluded to the dataset given in input to the algorithm as well as channel 1 (sensor 2) due to a malfunction of the piezo sensor. The signal available from the post analysis was related to channel 0 (sensor 1) and considering the required number of sensors by the algorithm to be able to estimate the location of the impact, results for this test were not produced. In Figure 12, below, the failed sensors are not reported.

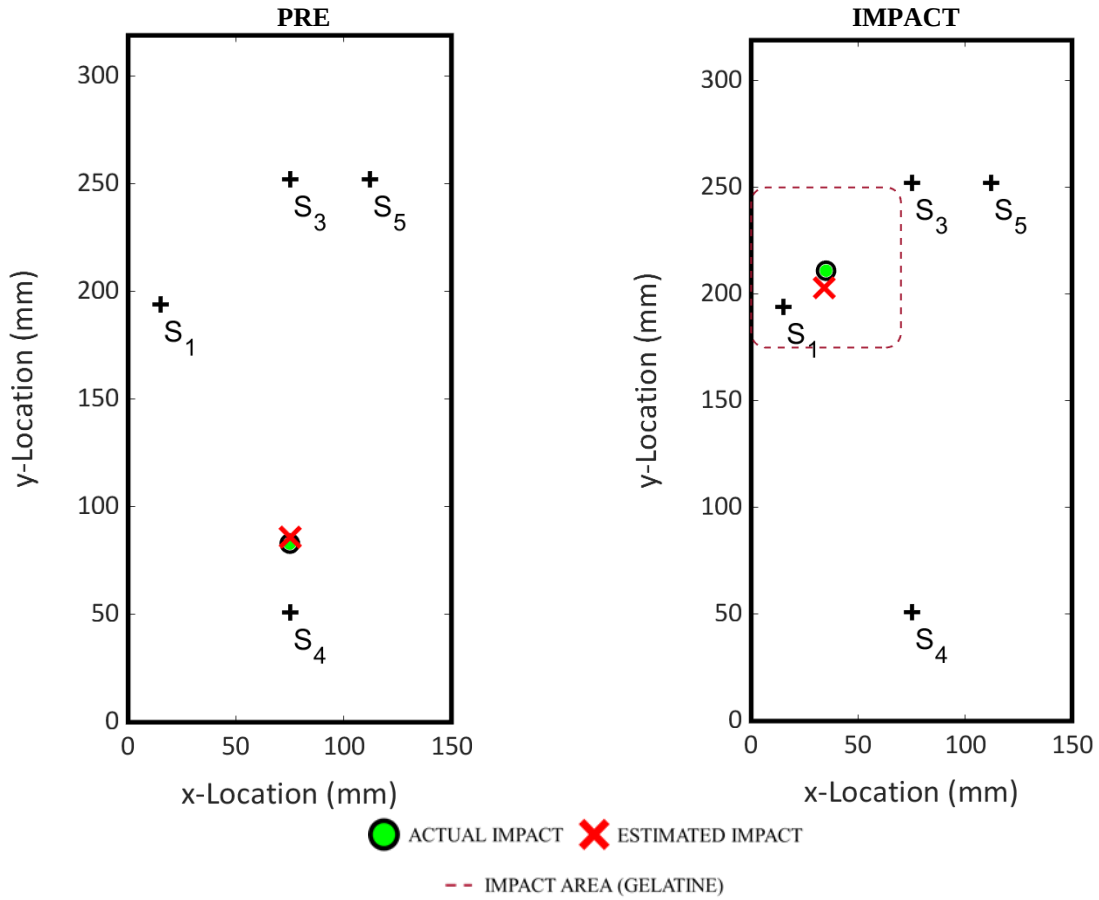

Figure 12. Impact location estimation 190 m/s, pre analysis (**PRE**) and impact with gelatine (**IMPACT**).

In pre analysis sensors 2 and 6 were not useful for the localisation of the impact for the aforementioned reason, but good accuracy was achieved though, with an error around 3 mm with four operating receivers. The localisation with data from the impact with the gelatine block was performed with only four working sensors (1-3-4-5) because numbers 2 and 6 were faulty. Even though the accuracy was remarkable with localisation error Λ around 8 mm. Unfortunately, data acquired in post analysis were badly affected by the previous high velocity impact, indeed only one sensor (channel 0) was functioning, hence no localisation is available for this test. The high energy induced by the impact caused damage on the sensing layer, as confirmed by the capacitance measurements executed after the impact.
Results from the second impact scenario show good accuracy of the proposed method even for high velocities. Moreover, the algorithm is capable of locating the impact even when some sensors of the sensing layer are faulty, indeed as depicting in Fig. 12 (right), with only four sensors available, the localisation is still accurate. This test confirms the discussion about the manufacturing and application of the sensing layer, and how to improve it, to achieve a robust sensing system. An approach for robust manufacturing process is given in [38], [39]. Results confirm the validity of the proposed localisation technique.
In Table 2 are reported localisation results from the test executed in this experimental campaign.

LOCALISATION ERROR Λ [mm]					
90 m/s			190 m/s		
PRE	IMPACT	POST	PRE	IMPACT	POST
11.60	4.61	16.73	2.81	7.96	/

Table 2 – Localisation error: 90 m/s and 190 m/s.

In Fig. 13, the representation of the signal power distribution obtained after the application of the RBF method, is depicted on the blade, as well as the localisation, for the 90 m/s scenario.

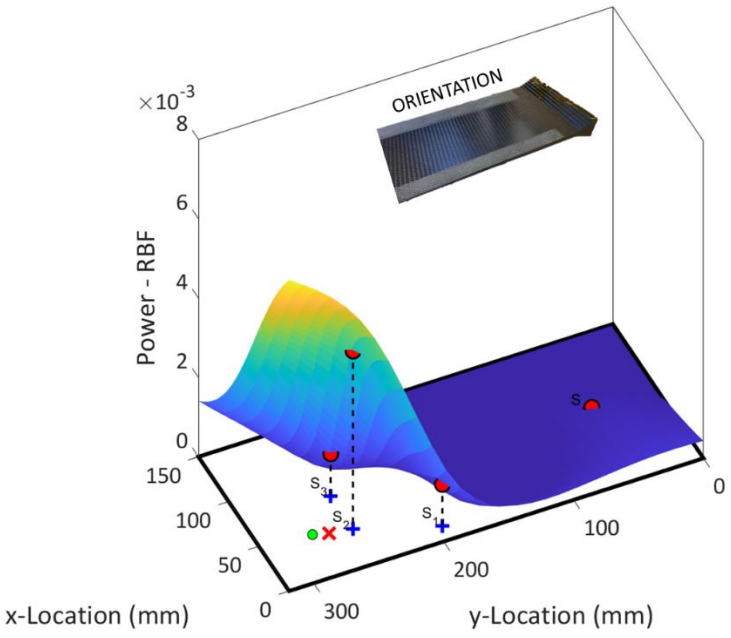

Figure 13. Power distribution with RBF interpolation.

6. DAMAGE ASSESMENT

In this section, the authors included a damage analysis of the blade, with a novel assessment method proposed in [40] that exploits the Hilbert-Huang Transform (HHT) of the decomposed wave modes. The technique is based

on the assumption that as long as damage is induced into a structure, the modes of the propagating waves are modified, and specifically the extensional mode more becomes predominant respect to the flexural mode.
Once the signals are acquired from the sensing network, usually made of piezo sensors, the algorithm process the data to perform the mode decomposition in order to obtain the two fundamental modes, extensional and flexural. The empirical mode decomposition (EMD) is applied for the previous task, and the output are the intrinsic mode functions (IMF). The mode extraction is executed considering a reference wave phase velocity, and evaluating the instantaneous wavelength:

$$\lambda_i = \frac{c}{f_i} \tag{9}$$

known the latter, it is possible to extract from the IMF extensional and flexural components. Consequently, the Hilbert transform is applied on the retrieved data, obtaining the Hilbert spectrum and thus the instantaneous energy of the single mode. The Hilbert transform is given by the following [41]:

$$\mathcal{H}[x(t)] = \frac{P}{\pi} \int_{-\infty}^{+\infty} \frac{x(\tau)}{t-\tau} d\tau \tag{10}$$

P is the singular integral principal value. The analytical signal z(t) is the combination of the complex conjugate pair x(t) and y(t), thus[42]:

$$z(t) = x(t) + iy(t) = a(t)e^{i\theta(t)} \tag{11}$$

Where $a(t) = \sqrt{[x^2(t) + y^2(t)]}$ is the instantaneous amplitude and $\theta(t) = \arctan[\, y(t)/x(t)\,]$ is the phase function. The instantaneous frequency and instantaneous energy are derived by the followings:

$$\omega = \frac{d\theta}{dt} \qquad E_i = |a_i(t)|^2 \tag{12}$$

Extracted the wave mode features by the HHT, the parameter Ξ is introduced that identifies the damage state of the specimen under examination.
The parameter Ξ is defined as the following:

$$\Xi = \frac{Max\ E_{i_{extensional}}}{Max\ E_{i_{flexural}}} \tag{13}$$

The maximum instant energy values are extracted by the HHT, once mode decomposition is performed separating the flexural from the extensional mode.
From the analysis of the signal acquired during the impact with the ballistic gelatine at 90 and 190 m/s, the instant energy values are as follows:

	PRE	DURING 90	DURING 190
EXT	0.5865	0.1395	16.15746
FLEX	1.5941	217.4023	303.76335

Table 3 – Instant energy values for different test scenario.

Afterwards, the values of the proposed energy ratio Ξ are evaluated and reported in the bar plot below.

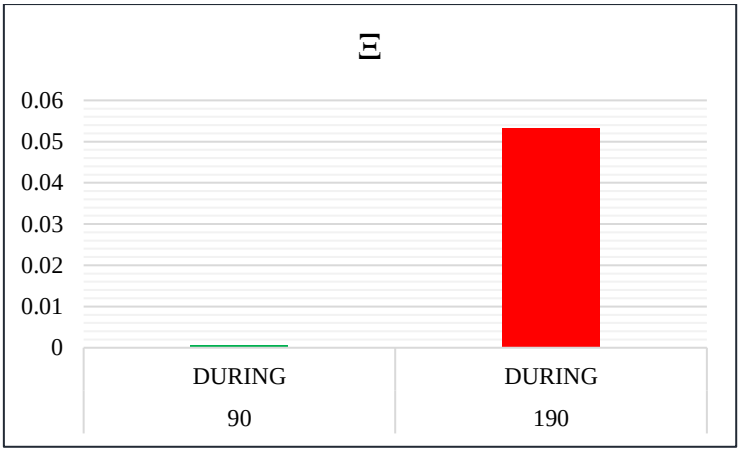

Figure 14. Ξ values for impact at 90 and 190 m/s.

From Figure 14 it's possible to observe how the damage induced to the blade modifies the instant energy distribution, modifying the Ξ parameter. As described in literature, a modification in the mode propagation is strictly related to the generation of damage into the structure [43], [44] and can be exploited to assess the presence of damage. From the values presented, it is possible to appreciate the considerable increment of the extensional mode outweighing the flexural mode. This agrees well with the common response observed in impacted composite plates subjected to low and high velocity impact [43], [45]. Compared to the results in [40], in this work it is not possible to relate the parameter to a specific type of damage, but rather give a qualitative assessment of integrity state of the specimen subjected to impact. This limit is due to the experimental setup, the projectile used, the complex geometry and stacking sequence of the specimen. Even though, the remark of this method it's the possibility to evaluate the damage condition without the need of baseline dataset as a reference.

7. CONCLUSIONS

In this paper, the signal power method was applied to determine the location of high velocity impact performed on a composite engine blade. Two velocity configurations were considered: at 90 and 190 m/s. The projectile used for each test were blocks of ballistic gelatine. The blade used during the experimental campaign was made of carbon fibre reinforced polymer and a complex stacking sequence with an embedded sensing layer fitted with six piezo elements. The tests performed were recorded with a high-speed camera system.

The first test demonstrated the ability of the method to locate the impact performed at high velocity, with an error in the estimation below 5 mm (from the centre of the area affected by the impacting projectile). The capability of the developed algorithm was confirmed by the PRE and POST test executed with modal hammer, showing that even at very low energy levels, the method was still effective. Nevertheless, the pre and post analyses were executed to confirm the integrity state of the sensing layer. This was in good agreement with the capacitance measurements executed on the piezo elements.

The second test was a confirmation of the consistency of the proposed location method, with a good estimation of the point of the impact with an error around 8 mm (from the centre of the area affected by the impacting projectile). In this case the impact localisation performance is enhanced because before the execution of the actual impact, capacitance measurements demonstrated that only 4 out of 6 piezo elements were operative. Moreover, considering the high level of energy of the second test, 3 piezo elements went to complete failure. Infeed, only the first wave packet was considered to run the location estimation.

The proposed method is effective in the estimation of the location for different impact scenarios, from low to high velocity impact, overcoming the common limitations of previous techniques such as a priori knowledge of mechanical properties, vibration response analysis, wave propagation direction dependency, sensor locations, and the necessity of a baseline.

Exploiting a novel technique, based on the Hilbert-Huang transform and mode decomposition, the damage assessment of the blade was executed using data from the high velocity impact signals. The proposed method evaluates the instant energy of the decomposed extensional and flexural modes of the propagating waves and

gives in output a parameter defined as the maximum energy ratio of the aforementioned modes. From the results, it is clear how the parameter synthesises the modification that occurs when damage is induced to the structure, thus when one mode becomes more predominant than the other. In good agreement with previous findings in literature, at the highest velocity test, there is a clear sign of mode modification, where the extensional component share increases and the flexural one is reduced. The sign of damage on the blade is clear from the high-speed records, with delamination visible from the top edge of the sample.

REFRENCES

[1] "Guidelines for Implementation of Structural Health Monitoring on Fixed Wing Aircraft." SAE, 2013.

[2] V. Giurgiutiu, "Introduction," in *Structural Health Monitoring with Piezoelectric Wafer Active Sensors*, Elsevier, 2014, pp. 1–19.

[3] T. Kundu, "Acoustic source localization," *Ultrasonics*. 2014.

[4] V. Giurgiutiu, "Structural health monitoring with piezoelectric wafer active sensors," in *16th International Conference on Adaptive Structures and Technologies*, 2006.

[5] S. Metaxa, K. Kalkanis, C. S. Psomopoulos, S. D. Kaminaris, and G. Ioannidis, "A review of structural health monitoring methods for composite materials," *Procedia Struct. Integr.*, vol. 22, no. 2019, pp. 369–375, 2019.

[6] M. Abbas and M. Shafiee, "Structural health monitoring (SHM) and determination of surface defects in large metallic structures using ultrasonic guided waves," *Sensors (Switzerland)*, vol. 18, no. 11, 2018.

[7] C. Kralovec and M. Schagerl, "Review of structural health monitoring methods regarding a multi-sensor approach for damage assessment of metal and composite structures," *Sensors (Switzerland)*, vol. 20, no. 3, pp. 1–25, 2020.

[8] A. Tobias, "Acoustic-emission source location in two dimensions by an array of three sensors," *Non-Destructive Test.*, 1976.

[9] T. Kundu, S. Das, S. A. Martin, and K. V. Jata, "Locating point of impact in anisotropic fiber reinforced composite plates," *Ultrasonics*, 2008.

[10] G. C. McLaskey, S. D. Glaser, and C. U. Grosse, "Beamforming array techniques for acoustic emission monitoring of large concrete structures," *J. Sound Vib.*, vol. 329, no. 12, pp. 2384–2394, 2010.

[11] T. He, Q. Pan, Y. Liu, X. Liu, and D. Hu, "Near-field beamforming analysis for acoustic emission source localization," *Ultrasonics*, vol. 52, no. 5, pp. 587–592, 2012.

[12] H. Nakatani, T. Hajzargarbashi, K. Ito, T. Kundu, and N. Takeda, "Impact localization on a cylindrical plate by near-field beamforming analysis," in *Sensors and Smart Structures Technologies for Civil, Mechanical, and Aerospace Systems 2012*, 2012.

[13] H. Nakatani, T. Hajzargarbashi, K. Ito, T. Kundu, and N. Takeda, "Locating point of impact on an anisotropic cylindrical surface using acoustic beamforming technique," in *Key Engineering Materials*, 2013.

[14] F. Ciampa and M. Meo, "A new algorithm for acoustic emission localization and flexural group velocity determination in anisotropic structures," *Compos. Part A Appl. Sci. Manuf.*, 2010.

[15] F. Ciampa, M. Meo, and E. Barbieri, "Impact localization in composite structures of arbitrary cross section," *Struct. Heal. Monit.*, 2012.

[16] T. Kundu, "A new technique for acoustic source localization in an anisotropic plate without knowing its material properties," in *Proceedings of the 6th European Workshop - Structural Health Monitoring 2012, EWSHM 2012*, 2012.

[17] M. E. De Simone, F. Ciampa, S. Boccardi, and M. Meo, "Impact source localisation in aerospace composite structures," *Smart Mater. Struct.*, 2017.

[18] R. K. Ing, N. Quieffin, S. Catheline, and M. Fink, "In solid localization of finger impacts using acoustic time-reversal process," *Appl. Phys. Lett.*, 2005.

[19] F. Ciampa and M. Meo, "Impact detection in anisotropic materials using a time reversal approach," *Struct. Heal. Monit.*, 2012.

[20] F. Ciampa and M. Meo, "Impact localization on a composite tail rotor blade using an inverse filtering approach," *J. Intell. Mater. Syst. Struct.*, 2014.

[21] F. Ciampa, S. Boccardi, and M. Meo, "Factors affecting the imaging of the impact location with inverse filtering and diffuse wave fields," *J. Intell. Mater. Syst. Struct.*, 2016.

[22] M. E. De simone, F. Ciampa, and M. Meo, "A hierarchical method for the impact force reconstruction in composites structures," *Smart Mater. Struct.*, 2018.

[23] S. Cuomo, M. E. De Simone, C. Andreades, F. Ciampa, and M. Meo, "Machine learning for impact detection on composite structures," *Mater. Today Proc.*, no. xxxx, pp. 1–6, 2020.

[24] A. Coles, B. A. de Castro, C. Andreades, F. G. Baptista, M. Meo, and F. Ciampa, "Impact Localization in Composites Using Time Reversal, Embedded PZT Transducers, and Topological Algorithms," *Front. Built Environ.*, vol. 6, no. March, pp. 1–14, 2020.

[25] J. Park, S. Ha, and F. K. Chang, "Monitoring impact events using a system-identification method," *AIAA J.*, vol. 47, no. 9, pp. 2011–2021, 2009.

[26] M. E. De Simone *et al.*, "Acoustic emission localization in composites using the signal power method and embedded transducers," 2019.

[27] S. Cuomo, G. P. M. Fierro, and M. Meo, "Damage localization on composite structures: radial basis function application," no. April, p. 12, 2020.

[28] F. Ciampa, S. G. Pickering, G. Scarselli, and M. Meo, “Nonlinear imaging of damage in composite structures using sparse ultrasonic sensor arrays,” *Struct. Control Heal. Monit.*, 2017.
[29] M. D. Buhmann and J. Levesley, “Radial Basis Functions: Theory and Implementations,” *Math. Comput.*, 2004.
[30] M. Buhmann, “Radial basis function,” *Scholarpedia*, vol. 5, no. 5, p. 9837, 2010.
[31] M. Mongillo, “Choosing Basis Functions and Shape Parameters for Radial Basis Function Methods,” *SIAM Undergrad. Res. Online*, 2011.
[32] S. Nitschke, A. Hornig, A. Winkler, and N. Modler, “Tailored embeddable sensor-actuator layers for CFRP aerospace structures,” *10th Int. Symp. NDT Aerosp.*, pp. 1–10, 2018.
[33] M. Hornig, A.; Frohberg, R.; Bätzel, T.; Nitschke, S.; Modler, N.; Gude, “‘Publication Pending,’” *Pending*.
[34] M. Bauerfeind, E.; Hornig, A.; Weck, W.A.D.; Modler, N.; Gude, “Delamination behaviour of embedded polymeric sensor and actuator carrier layers in epoxy based CFRP laminates - A study of energy release rates (PENDING),” *Pending*.
[35] U. K. Vaidya, “Impact response of laminated and sandwich composites,” *CISM Int. Cent. Mech. Sci. Courses Lect.*, vol. 526, pp. 97–191, 2011.
[36] S. Abrate, “Impact on Laminated Composite Materials,” *Appl. Mech. Rev.*, vol. 44, no. 4, p. 155, 1991.
[37] P. Robinson and G. A. O. Davies, “Impactor mass and specimen geometry effects in low velocity impact of laminated composites,” *Int. J. Impact Eng.*, 1992.
[38] A. . Hornig, R. . Frohberg, T. . Bätzel, M. Gude, and N. . Modler, “Embedded Sensing and Actuating in CFRP Composite Structures - Concept and Technology Demonstration for Tailored Embeddable Sensor-Actuator Layers (TEmSAL),” *Smart Mater. Struct.*, vol. Pending, 2022.
[39] A. Hornig, A. Winkler, E. Bauerfeind, M. Gude, and N. Modler, “Delamination behaviour of embedded polymeric sensor and actuator carrier layers in epoxy based cfrp laminates—a study of energy release rates,” *Polymers (Basel).*, 2021.
[40] S. Cuomo, M. Boccaccio, and M. Meo, “Damage identification during an impact event using the Hilbert-Huang transform of decomposed propagation modes,” *Pending*, vol. Pending.
[41] N. E. Huang and S. S. P. Shen, *Hilbert-huang transform and its applications*. 2005.
[42] N. E. Huang *et al.*, “The empirical mode decomposition and the Hubert spectrum for nonlinear and non-stationary time series analysis,” *Proc. R. Soc. A Math. Phys. Eng. Sci.*, 1998.
[43] W. H. Prosser, M. R. Gorman, and D. H. Humes, “Acoustic Emission Signals in Thin Plates Produced by Impact Damage,” *J. Acoust. Emiss.*, vol. 17(1–2), no. June 1998, pp. 29–36, 1999.
[44] H. Mei, M. F. Haider, R. James, and V. Giurgiutiu, “Pure S0 and SH0 detections of various damage types in aerospace composites,” *Compos. Part B Eng.*, 2020.
[45] W. H. Prosser and M. R. Gorman, “Plate mode velocities in graphite/epoxy plates,” *J. Acoust. Soc. Am.*, vol. 96, no. 2, pp. 902–907, 1994.